Mechanism of thermal conductivity suppression in doped silicon studied with nonequilibrium molecular dynamics

Yongjin Lee and Gyeong S. Hwang*
Department of Chemical Engineering, University of Texas, Austin, Texas 78712, USA
(Received 27 May 2012; published 7 August 2012)

We examined the underlying mechanisms for thermal conductivity suppression in crystalline silicon by substitutional doping with different elements (X = boron, aluminum, phosphorus, and arsenic). In particular, the relative effects of doping-induced mass disorder, bond disorder, and lattice strain were assessed using nonequilibrium molecular dynamics simulations. Stillinger–Weber potential parameters for Si-X interatomic interactions were optimized by fitting to relevant atomic forces from first-principles calculations. We first calculated the thermal conductivity variation of B-doped Si as a function of dopant concentration; the result shows excellent agreement with existing experimental data, indicating the reliability of our force-field-based simulations. At the dopant concentration of about 5×10^{20} cm^{-3}, the Si thermal conductivity value is predicted to be reduced from 137 W/mK at 300 K in undoped Si to 18/39/57/78 W/mK in As/B/P/Al-doped Si. Our study demonstrates that the mass disorder effect is primarily responsible for the thermal conductivity suppression in the As- and B-doped cases, whereas the bond disorder contribution is found to be more important than the mass disorder contribution in the Al- and P-doped cases; for all these systems, the lattice strain effect turns out to play a minor role in the reduction of lattice thermal conductivity.

DOI: 10.1103/PhysRevB.86.075202 PACS number(s): 65.40.−b

I. INTRODUCTION

Thermoelectric devices that directly convert heat energy to electricity and vice versa have recently attracted renewed interest for their potential applications ranging from household power to spacecraft.[1–4] The efficiency of a thermoelectric device is usually quantified by the dimensionless figure of merit ($ZT = S^2\sigma T/\kappa$, where S is the Seebeck coefficient, σ is the electrical conductivity, κ is the thermal conductivity, and T is the absolute temperature).[5] Various candidate materials, such as nanostructured compound semiconductors,[6–8] have been explored, but today's thermoelectric materials are still very expensive to synthesize and not yet efficient enough to be commercially viable. Although bulk crystalline silicon (c-Si) exhibits very poor thermoelectric performance ($ZT \sim 0.01$)[9] due to its high thermal conductivity, there has been a continued interest in Si-based thermoelectric materials because they are cheap and easy to work with and have good modifiable electrical properties for thermoelectric applications.

Much research[1,2,10–14] has been directed towards finding ways to reduce the thermal conductivity of Si-based materials to increase ZT. While heat conduction in Si is mainly governed by phonon transport, recently, many attempts have been made to suppress the thermal conductivity by introducing phonon scattering through nanostructuring, doping, and alloying.[15–18] Phonon-boundary scattering has been found to bring about a substantial reduction of thermal conductivity in Si nanostructures, such as nanowire and thin film. In addition, the presence of isotopes, intrinsic lattice defects, and chemical impurities in Si would lead to scattering of phonons, which can in turn significantly influence thermal conductivity suppression. For instance, previous studies have demonstrated that the thermal conductivity of Si nanowires with 50% isotope atoms can be reduced up to about 27% of that of pure ^{28}Si nanowires,[19] and the presence of a small concentration (∼1.5%) of vacancies can bring about an almost 95% reduction of bulk Si thermal conductivity at 300 K.[20] In addition, the thermal conductivity of Si can be effectively reduced by impurity doping or alloying. It has been suggested that the mass difference between Si and Ge (the so-called mass disorder effect) may play an important role in thermal conductivity suppression in SiGe alloys.[21] However, the underlying atomic-level mechanism of doping/alloying-induced phonon-impurity scattering in Si-based materials is not yet fully clarified.

In this paper, we perform a quantitative analysis of the effects of dopants on phonon transport in c-Si, particularly the underlying mechanisms of phonon scattering due to different types of dopants, including boron (B), aluminum (Al), phosphorous (P), and arsenic (As). Previous experimental studies[22–25] have demonstrated that the effect of different dopant species (B, P, As) on thermal conductivity reduction tend to vary substantially. However, only a very limited amount of effort has been undertaken to address explicitly the roles played by dopants in the phonon-impurity scattering. To our knowledge, most of the earlier theoretical investigations[22,23,25] have focused on explaining the variation of thermal conductivity with temperature and dopant concentration based on Klemens formula[26] and Holland model,[27] not the specific contributions of different dopants. Motivated by this, this paper attempts to address the underlying causes of phonon-impurity scattering for different types of dopants, especially related to the mass disorder, bond disorder, and lattice strain induced by dopant incorporation. Nonequilibrium molecular dynamics (NEMD)[28] with the Stillinger–Weber (SW) potential model[29] is adopted to calculate the thermal conductivities of doped Si systems; the SW parameters are modified based on the first-principles-based force-matching method.[30]

II. THEORY

A. Nonequilibrium molecular dynamics

Following Fourier's law ($\kappa = -J/\Delta T$), thermal conductivity (κ) can be obtained by calculating a temperature

gradient (ΔT) for an imposed heat flux (J), or vice versa, from a NEMD simulation. We performed NEMD simulations using large-scale atomic and molecular massively parallel simulator (LAMMPS).[31] The MD temperature (T_{MD}) was calculated from the velocities of constituent atoms based on the equipartition theorem of classical statistical mechanics: $\frac{3}{2}Nk_BT_{MD} = \frac{1}{2}\sum_{i=1}^{N} mv_i^2$, where N is the number of atoms in a system, k_B is the Boltzmann constant, v_i is the velocity of atom i, and m is the atomic mass. If T_{MD} is below the Debye temperature (T_D), quantum corrections to T_{MD} and κ_{MD} are necessary; the correction can be made by $\kappa = \kappa_{MD}\frac{dT_{MD}}{dT}$.[32] (All κ values reported hereafter are after quantum corrections, unless stated otherwise). In this paper, doped Si systems considered were assumed to have the same T_D as Si (=645 K[33]), as the atomic fractions of dopants are very small (<0.01); note that the Debye temperature of an alloy system ($A_{1-x}B_x$) is typically approximated by the linear relation of $T_D(AB) = (1-x)T_D(A) + xT_D(B)$.[34]

B. Force-matching-based SW parameter optimization

For NEMD simulations, we employed a general form of SW potential function which includes two-body (stretching) and three-body (bending) terms. The SW parameters were optimized for Si-X (X = B, P, As, or Al) systems using a force-matching method[35] based on DFT calculations of the restoring forces associated with atomic displacements. The force-matching-based parameterization has been demonstrated to be a reliable choice for calculation of the lattice thermal conductivities of Si-based materials;[30,36] more details regarding the force-matching approach can be found in Ref. 30.

The DFT force data for the parameter optimization were obtained by displacing a dopant atom or its neighboring atoms in the x, y, and z directions by 0.08 Å. The restoring forces acting on the displaced atom and its four first-nearest neighbors were considered to be matched in the SW parameter adjustments. On the third-nearest neighbors and beyond, the forces due to the center-atom displacement turn out to be negligible (less than 0.01 eV/Å in the absolute value). In this paper, the force constants for the second-nearest Si neighbors and beyond were assumed to be the same as those for c-Si; although the second-nearest Si atoms have three-body interactions with the dopant atom (Si-Si-X), the contribution is likely to be insignificant. The optimal values for a, ε, and λ were obtained by minimizing the cross-validation error (ξ); $\xi^2 = \frac{1}{N}\sum_{n=1}^{N}[F_{DFT}^{(n)} - F_{SW}^{(n)}]^2$, where $F_{DFT}^{(n)}$ and $F_{SW}^{(n)}$ refer to the DFT and SW forces, respectively, of the nth of N total training data for force matching.

Our DFT calculations were performed within the Perdew–Wang 91 generalized gradient approximation (GGA-PW91),[37] using the Vienna *ab initio* simulation package (VASP).[38] We used Vanderbilt-type ultrasoft pseudopotentials[39] to represent the interaction between ion cores and valence electrons, and a plane-wave basis set with a kinetic energy cutoff of 250 eV. We used a 64-atom cubic supercell that contains one dopant atom and 63 Si atoms for optimizing Si-dopant interaction potentials. A $(2 \times 2 \times 2)$ k-point grid in the scheme of Monkhorst–Pack was used for the Brillouin zone sampling.

Table I summarizes the modified parameters from the force matching approach; the σ values were chosen to match the Si-X bond distances (X = B, Al, P, As) from DFT-GGA calculations. In addition, the equilibrium Si-Si-X bond angles (θ_0) were obtained from DFT-GGA calculations, while the equilibrium Si-Si-Si and Si-X-Si bond angles were set at 109.47° (tetrahedral bond angle). Figure 1 shows the comparisons of the restoring forces from our SW and DFT-GGA calculations; overall, the modified SW parameters provide excellent reproduction of corresponding DFT forces (acting on the center dopant atoms and their Si neighbors).

TABLE I. Modified parameters of the Stillinger–Weber interatomic potential [see Eqs. (2) and (3) in Ref. 30 for Si-X interactions (X = B, P, As, and As); σ, ε, λ, a, and cos θ_0 values were optimized based on DFT-GGA calculations of local lattice structure and restoring forces arising from local lattice distortions.

	Si-B	Si-P	Si-Al	Si-As
σ	1.8675	2.0994	2.1483	2.1702
ε (eV)	1.2496	1.0235	1.4858	1.0772
λ	33.8815	64.3998	17.5472	49.9274
a	1.6452	1.8003	1.8379	1.8688
cos θ_0	− 0.4195	− 0.3298	− 0.3251	− 0.3036
$A = 7.049556277$, $B = 0.6022245584$, $p = 4.0$, $q = 0.0$, and $\gamma = 1.2$.				

III. RESULTS AND DISCUSSION

A. Comparison with experiments for B-doped Si

To assess the reliability of the SW interatomic potential with modified parameters, we compared calculated κ values with existing experimental data for bulk c-Si doped with B at various doping concentrations. For NEMD simulations, as illustrated in Fig. 2, we used a periodic rectangular cell which consists of the heat source (S_H) and heat sink (S_C) layers, two intermediate (I) layers, and two buffer (B) layers. The cross section of the simulation cell consists of 10 × 10 units (corresponding to 400 atoms). The S_H/S_C and B layer thicknesses were set at L_S = 5.4571 Å and L_B = 54.571 Å [corresponding to one (or 400 atoms) and 10 units, respectively, in the axial ⟨100⟩ direction], while L_I was varied depending on simulation cell size. Dopant atoms were assumed to remain isolated without making any pairs or larger clusters, and they were placed in a random manner in the simulation domain; the dopant concentrations in the S_H/S_C, B, and I layers were controlled to be (nearly) equal.

Figure 3 shows predicted κ values for B-doped bulk c-Si at B concentrations of n_B = 1.21875, 2.4375, 4.875, and 7.3125×10^{20} atoms/cm^3 (corresponding to the atomic percentages of x_B = 0.25, 0.5, 1, and 1.5 at.%, respectively). For comparison, the experimental data available from the published literature are also plotted. Note that each bulk κ value was obtained through extrapolation of finite-sized results to infinite size, as shown in the inset (here, $L_z = 1/2\ L_{\text{tot}}$); refer to Ref. 20 for a more detailed description of the computational technique. For a given simulation cell size and dopant-concentration system, we performed 25 independent NEMD simulations considering five different atomic-level spatial distributions of dopants, for each of which five different initial velocity distributions were also taken into account.

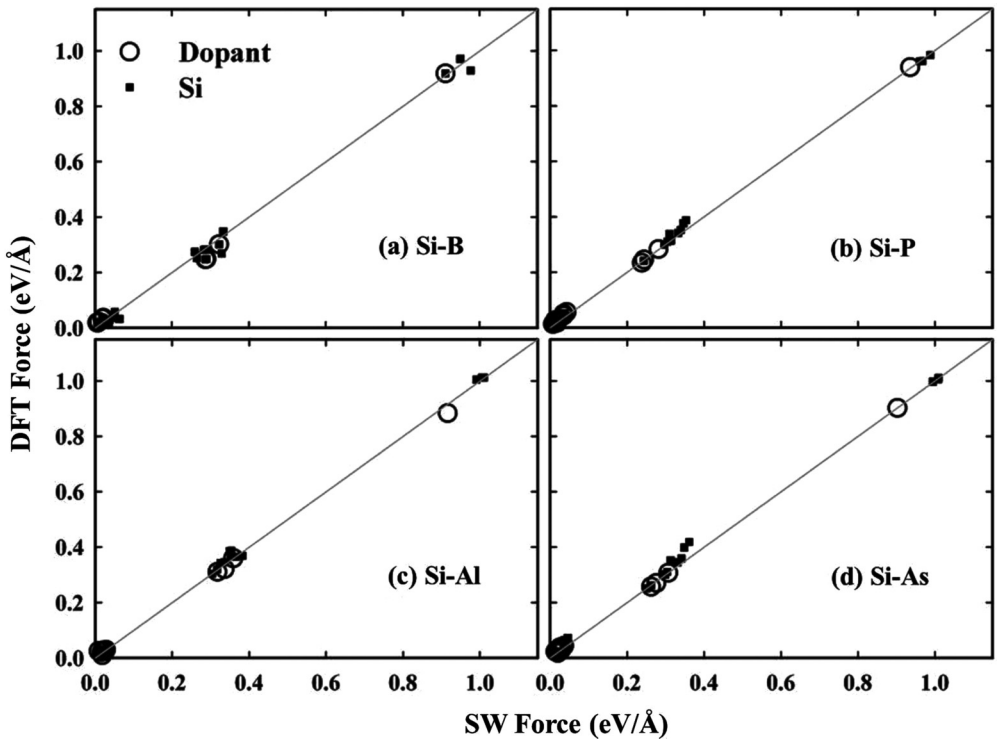

FIG. 1. Comparison between predicted DFT and SW forces acting on the displaced dopant atom and its four first-nearest Si atoms for four different doped systems as indicated.

The calculated κ values (after quantum corrections) are well fitted by $\kappa = \kappa_{Si}/(1 + A\bar{n}_B^{\alpha})$ with $A = 0.74186$ and $\alpha = 0.7411$, where κ_{Si} is the thermal conductivity of undoped c-Si (=136.65 $\mathrm{Wm^{-1}K^{-1}}$), and $\bar{n}_B$ is the dimensionless B concentration ($=n_B/10^{20}$ $\mathrm{cm^{-3}}$); the inverse power-law relationship has been widely adopted to describe the effect of point-like impurities (or defects) on lattice thermal conductivity.[19,20,40,41] We can see that the predicted value of $39.27 \pm 5.54\,\mathrm{Wm^{-1}K^{-1}}$ (at $n_B = 4.875 \times 10^{20}/\mathrm{cm^3}$) is very close to the experimentally reported value of 40 $\mathrm{Wm^{-1}K^{-1}}$ (at $n_B \approx 5 \times 10^{20}/\mathrm{cm^3}$).[42] In addition, the fitted relation shows good agreement with the experiment data of about 50 $\mathrm{Wm^{-1}K^{-1}}$ at $n = 3 \times 10^{20}/\mathrm{cm^3}$ and 18.5 $\mathrm{Wm^{-1}K^{-1}}$ at $n = 1.6 \times 10^{21}/\mathrm{cm^3}$. The excellent agreement between the simulation and experiment results increases our confidence in the validity of the modified SW parameters for use of estimating the lattice thermal conductivity of doped c-Si at moderate temperatures.

B. Comparison between B-, Al-, P-, and As-doped Si systems

1. Relative effectiveness in thermal conductivity suppression

Using the same NEMD approach as described in the previous Sec. III A, we examined how different substitutional dopants (B, Al, P, and As) affect the κ of c-Si. Since our intention was to compare the impurity scattering strengths

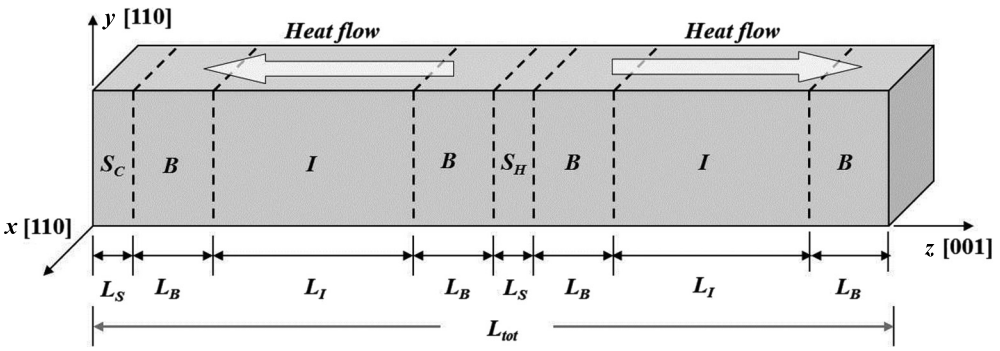

FIG. 2. Schematic illustration of a rectangular-shaped simulation domain with periodic boundary conditions imposed in the x, y, and z directions. The simulation cell consists of heat source (S_H), two heat sink (S_C), buffer (B), and intermediate (I) layers; temperature gradients used for thermal conductivity calculation were obtained only from the I layers to avoid any unwanted effects arising from velocity switching-induced nonphysical phonon scatterings in the S_H and S_C regions. Heat flows in two directions due to the periodic boundary condition imposed in the ⟨100⟩ direction, as indicated

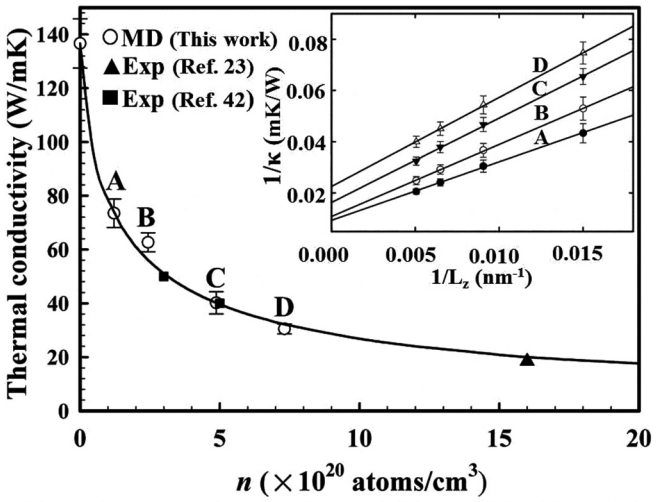

FIG. 3. Calculated bulk thermal conductivities of B-doped Si at 300 K as a function of dopant concentration (n_B), together with available experimental data for comparison. The solid line indicates a fitted curve to the simulation result, which is $\kappa = \kappa_{Si}/[1 + A(\frac{n_B}{10^{20}})^{\alpha}]$ with $A = 0.74186$, $\alpha = 0.7411$, and $\kappa_{Si} = 136.65$ $Wm^{-1}K^{-1}$. The inset shows thermal resistivity ($1/\kappa$, after quantum corrections) for B-doped Si at different doping concentrations as specified; for each set, the linear line indicates the best-fit linear regression. Here, Lz is the distance between the heat source and heat sink centers, which is half of the total simulation cell length (L_{tot}; see Fig. 2).

among those doped systems, here, we considered only a doping concentration of $n = 4.875 \times 10^{20}/cm^3$. For different doped systems, dopants were placed at the same sites to avoid any possible unwanted effect associated with the disparity between their spatial distributions. Compared to the undoped case ($\kappa_{Si} = 136.65 \pm 9.15$ W/mK), the introduction of Al, P, B, and As dopants leads to a considerable reduction in κ; as summarized in Fig. 4, the calculated ordering is $\kappa_{SiAl}(total) = 78.18 \pm 6.85 > \kappa_{SiP}(total) = 56.73 \pm 5.21 > \kappa_{SiB}(total) = 39.27 \pm 5.54 > \kappa_{SiAs}(total) = 18.32 \pm 2.17$ W/mK. Our simulations clearly demonstrate that As and B doping can more effectively suppress thermal transport in c-Si compared to P and Al. Overall, the simulation results are consistent with existing experimental observations. For instance, according to Liu *et al.*,[22] κ_{SiP} appears to be about twice larger than κ_{SiAs} when $n = 2.3 \times 10^{20}/cm^3$; in addition, Asheghi *et al.*[23] demonstrated that B doping tends to cause a greater suppression of κ than P doping.

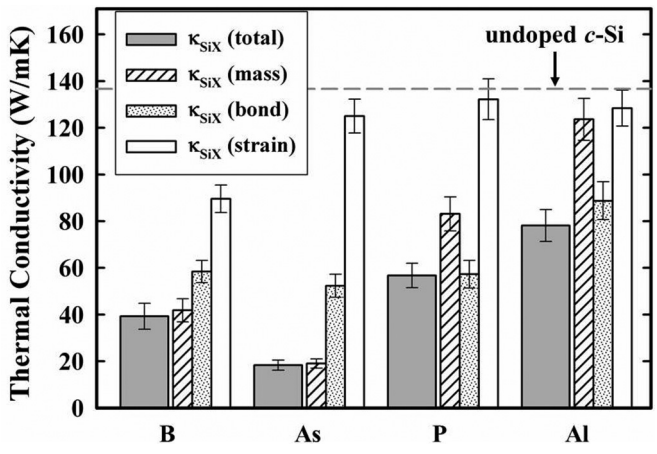

FIG. 4. Calculated thermal conductivities (after quantum corrections) for bulk c-Si doped with B, As, P, and Al at $T = 300$ K and $n = 4.875 \times 10^{20}/cm^3$. The dashed horizontal line indicates the predicted κ value of undoped Si (=136.65 $Wm^{-1}K^{-1}$). For each doped system, besides its bulk value [indicated as $\kappa_{SiX}(total)$], the κ values calculated by isolating each of the effects of mass disorder [$\kappa_{SiX}(mass)$], bond disorder [$\kappa_{SiX}(bond)$], and lattice strain [$\kappa_{SiX}(strain)$] are also plotted.

2. *Relative contributions of mass disorder, bond disorder, and lattice strain*

Phonon scattering by substitutional dopants can be attributed to the atomic mass and/or atomic radius differences between the host and dopant atoms; the mass and radius disparities are, respectively, related to the so-called mass disorder and lattice strain effects. In addition, the existence of the heterobonds between dissimilar (host and dopant) atoms may cause phonon scattering (the so-called bond disorder effect). Next, we discuss the relative contributions of mass disorder, bond disorder, and lattice strain to the κ suppression in each doped system.

Mass disorder effect. The effect of mass disorder was examined by assuming that dopant atoms have the same radius and force constants as Si (see Table I), but they have their own masses ($m_B = 10.81$, $m_{Al} = 26.98$, $m_P = 30.97$, $m_{As} = 74.92$, $m_{Si} = 28.08$); that is, the contributions of bond disorder and lattice strain were excluded. Here, dopant atoms were located at the same sites in the simulation cell as described in the previous Subsec. B1.

As summarized in Fig. 4, the κ suppression is more enhanced with increasing the ratio of mass difference ($\Lambda = |m_{Si} - m_X|/m_{Si}$, X = B, Al, P, As); the order from lowest to highest is as follows, $\kappa_{SiAl}(mass) = 123.61 \pm 8.97$ $Wm^{-1}K^{-1}$ ($\Lambda = 0.039$) < $\kappa_{SiP}(mass) = 83.13 \pm 7.28$ $Wm^{-1}K^{-1}$ ($\Lambda = 0.103$) < $\kappa_{SiB}(mass) = 41.82 \pm 4.98$ $Wm^{-1}K^{-1}$ ($\Lambda = 0.615$) < $\kappa_{SiAs}(mass) = 19.05 \pm 1.98$ $Wm^{-1}K^{-1}$ ($\Lambda = 1.668$). The simulation results advocate well the model suggested by Abeles for the alloy scattering strength (Γ) due to mass difference;[43] $\Gamma \propto [\frac{(1-x_i)M_i - (1-x_i)M_h}{x_i M_i + (1-x_i)M_h}]^2$, where x_i and M_i are the fractional concentration and the mass of the impurity atom, and M_h is the mass of the host atom; if $x_i \ll 1$, $\Gamma \propto (\frac{M_i - M_h}{M_h})^2 = \Lambda^2$.

For As, $\kappa_{SiAs}(mass)$ (=19.05 $Wm^{-1}K^{-1}$) is very close to $\kappa_{SiAs}(total)$ (=18.32 $Wm^{-1}K^{-1}$), indicating that the mass disorder effect is primarily responsible for κ suppression in the As-doped system. Likely, in the B-doped case where the mass difference is also significant, the extent of κ reduction [$\Delta\kappa_{SiB}(mass) = \kappa_{Si} - \kappa_{SiB}(mass)$] due to mass disorder is predicted to be 94.83 (=136.65 − 41.82) $Wm^{-1}K^{-1}$, which is about 97% of the total reduction of 97.38 ($\Delta\kappa_{SiB}(total) = \kappa_{Si} - \kappa_{SiB}(total) = 136.65 - 39.27$) $Wm^{-1}K^{-1}$. On the other hand, the mass disorder contribution appears to be relatively insignificant for the Al- and P-doped cases, only about 22% and 67%, respectively.

Bond disorder effect. To look at the bond disorder effect, the masses and radii of dopant atoms were assumed to be the same as those of the host Si atom, while other force constants optimized for each doped system were used (see Table I). Our

calculations show that the κ reduction due to bond disorder can be significant for all four doped systems, following the order of [κ_{SiAl}(bond) = 88.74 ± 8.13 > κ_{SiB}(bond) = 58.41 ± 4.74 > κ_{SiP}(bond) = 57.26 ± 5.88 > κ_{SiAs}(bond) = 52.31 ± 4.96 $Wm^{-1}K^{-1}$]. Interestingly, for the Al- and P-doped cases, the bond disorder effect is found to be more important than the mass disorder effect; that is, $\Delta\kappa_{SiAl}$(bond) [= κ_{Si} − κ_{SiAl}(bond) = 47.91 $Wm^{-1}K^{-1}$] and $\Delta\kappa_{SiP}$(bond) [= κ_{Si} − κ_{SiP}(bond) = 79.39 $Wm^{-1}K^{-1}$] are about 82% and 99% of $\Delta\kappa_{SiAl}$(total) (=58.47 $Wm^{-1}K^{-1}$) and $\Delta\kappa_{SiP}$(total) (=79.92 $Wm^{-1}K^{-1}$), respectively.

In the three-body SW potential, the interatomic forces can be decoupled into two-body (F) and three-body (G) contributions; that is, $F \propto \frac{\varepsilon}{\sigma^2}$ and $G \propto \frac{\varepsilon\lambda}{\sigma^2}$, where σ, ε, and λ are SW parameters. Looking at the two- and three-body force components associated with dopant atoms, relative to the host Si lattice, we can notice that only the two-body contribution tends to be important for Al [γ_F(Al) = 1.005 and γ_G(Al) = 0.597], whereas both two- and three-body force disturbances play a comparably important role in causing phonon scattering in the B-, P-, and As-doped cases [γ_F(B) = 1.118, γ_G(B) = 1.283; γ_F(P) = 0.725, γ_G(P) = 1.581; γ_F(As) = 0.713, γ_G(As) = 1.207].

Lattice strain effect. We looked at the lattice strain effect by assuming that dopant atoms have the same mass and force constants as Si, except $\theta_{Si\text{-}Si\text{-}X}$ and $\sigma_{Si\text{-}X}$ (X = dopant). As summarized in Fig. 4, our calculations suggest that the doping-induced strain may play a minor role in suppressing the lattice thermal conductivity, particularly in the P- and As-doped systems (whose κ values are lower only by 3% and 9%, respectively, compared to the undoped Si reference). This is not surprising considering there is no significant dopant-induced local lattice distortion; note the small difference of length unit parameter between Si-dopant ($\sigma_{Si\text{-}P}$ = 2.0994, $\sigma_{Si\text{-}As}$ = 2.1702) and Si-Si ($\sigma_{Si\text{-}Si}$ = 2.1052, from our DFT-GGA calculations), and also that the bend angles of $\theta_{Si\text{-}Si\text{-}P}$ (=109.3°) and $\theta_{Si\text{-}Si\text{-}As}$ (=107.6°) are close to $\theta_{Si\text{-}Si\text{-}Si}$ (=109.5°°). Compared to Al, P, and As, B causes relatively more lattice distortions ($\theta_{Si\text{-}Si\text{-}B}$ = 114.8°) because of its smaller radius ($\sigma_{Si\text{-}B}$ = 1.8675) and thus leads to a larger strain effect; nonetheless, the contribution of lattice strain turns out to be far smaller than those of mass disorder and bond disorder.

Finally, it would be worth noting that the total reduction of κ is substantially less than the summation of those caused separately by mass disorder, bond disorder, and lattice strain. For instance, in the B-doped case, the total reduction [$\Delta\kappa_{SiB}$(total)] of 97.38 $Wm^{-1}K^{-1}$ is much smaller than 220.15 $Wm^{-1}K^{-1}$ [= $\Delta\kappa_{SiB}$(mass) (=94.83 $Wm^{-1}K^{-1}$) + $\Delta\kappa_{SiB}$(bond) (=78.24 $Wm^{-1}K^{-1}$) + $\Delta\kappa_{SiB}$(strain) (=47.08 $Wm^{-1}K^{-1}$)]. This can be explained by considering Matthiessen's rule which states that the total resistivity (τ_{tot}^{-1}) is the sum of the resistivities due to individual scattering sources, such as phonon-phonon (τ_{p-p}^{-1}), mass disorder ($\tau_{a,mass}^{-1}$), bond disorder ($\tau_{a,bond}^{-1}$), and lattice strain ($\tau_{a,strain}^{-1}$); that is, $\tau_{tot}^{-1} = \tau_{a,mass}^{-1} + \tau_{a,bond}^{-1} + \tau_{a,strain}^{-1} + \tau_{p-p}^{-1}$. As such, if one component is predominant, the other scattering effects become less important than the cases considered separately.

IV. SUMMARY

We examined the underlying causes of thermal conductivity suppression in substitutionally doped Si using NEMD simulations; here, four different dopant elements (X = B, Al, P, As) were considered. While heat conduction in Si is mainly governed by phonon transport, we analyzed especially the relative roles played by the differences in atomic mass (mass disorder) and atomic radius (lattice strain) as well as the hetero bonds (bond disorder) between host and dopant atoms in the thermal conductivity suppression of Si by doping-induced phonon-impurity scatterings. Nonequilibrium molecular dynamics simulations were performed using the three-body Stillinger–Weber (SW) potential model, and adjustable SW parameters were reoptimized for Si-X interatomic interactions by fitting to the restoring forces associated with atomic displacements from DFT calculations. With the modified SW parameters, we first assessed the thermal conductivity (κ) variation of B-doped Si with dopant concentration (n_B); the κ-n_B relation (after quantum corrections) is found to follow the inverse power law, $\kappa = \kappa_{Si}/[1 + A(\frac{n_B}{10^{20}})^{\alpha}]$ with A = 0.74186, α = 0.7411, and κ_{Si} = 136.65 $Wm^{-1}K^{-1}$. The simulation results show excellent agreement with existing experimental data, increasing our confidence in the force-field-based approach to estimate the lattice thermal conductivity of doped Si at moderate temperatures. At $n = 4.875 \times 10^{20}/cm^3$, our NEMD simulations predict the κ value to be reduced from 136.65 ± 9.15 (undoped Si) to 18.32 ± 2.17/39.27 ± 5.54/56.73 ± 5.21/78.18 ± 6.85 W/mK in As-/B-/P-/Al-doped Si. While the suppression of κ appears to be a strong function of dopant element, our calculations clearly demonstrate that the mass disorder effect is predominant in the As- and B-doped cases where the host-dopant mass difference is significant. On the other hand, the bond disorder effect is found to be substantially more important than the mass disorder effect in the Al- and P-doped cases. For these dopant elements considered, the contribution of lattice strain turns out to be far smaller than those of mass disorder and bond disorder. This study highlights the importance of not only mass disorder but also bond disorder in determining the κ of Si-based alloy materials. The improved understanding can provide insight into how to modify Si-based materials to enhance their thermoelectric properties through doping and/or alloying.

ACKNOWLEDGMENTS

We acknowledge the Robert A. Welch Foundation (F-1535) for their financial support. We would also like to thank the Texas Advanced Computing Center for use of their computing resources.

*Corresponding author: gshwang@che.utexas.edu

[1] A. I. Hochbaum, R. Chen, R. D. Delgado, W. Liang, E. C. Garnett, M. Najarian, A. Majumdar, and P. Yang, Nature **451**, 163 (2008).

[2] A. I. Boukai, Y. Bunimovich, J. Tahir-Kehli, and J. R. Heath, Nature **451**, 168 (2008).

[3] G. F. Snyder and E. S. Toberer, Nat. Mater. **7**, 105 (2008).

[4]Z. Shao, S. M. Haile, J. Ahn, P. D. Ronney, Z. Zhan, and S. A. Barnett, Nature **435**, 795 (2005).
[5]*CRC Handbook of Thermoelectrics*, edited by D. M. Rowe (CRC Press, Boca Raton, 1995), Ch. 5.
[6]R. Venkatasubramanian, E. Siivola, T. Colpitts, and B. O'Quinn, Nature **413**, 597 (2001).
[7]J. P. Heremans, V. Jovovic, E. S. Toberer, A. Saramat, K. Kurosaki, A. Charoenphakdee, S. Yamanaka, and G. J. Snyder, Science **321**, 554 (2008).
[8]P. F. P. Poudeu, J. D'Angelo, A. D. Downey, J. L. Short, T. P. Hogan, and M. G. Kanatzidis, Angew. Chem. Ind. Ed. **45**, 3835 (2006).
[9]L. Weber and E. Gmelin, Appl. Phys. A **53**, 136 (1991).
[10]D. Donadio and G. A. Galli, Phys. Rev. Lett. **102**, 195901 (2009).
[11]J. H. Lee, G. A. Galli, and J. C. Grossman, Nano Lett. **8**, 3750 (2008).
[12]J. H. Lee, J. C. Grossman, J. Reed, and G. A. Galli, Appl. Phys. Lett. **91**, 223110 (2007).
[13]W. Kim, J. Zide, A. Gossard, D. Klenov, S. Stemmer, A. Shakouri, and A. Majumdar, Phys. Rev. Lett. **96**, 045901 (2006).
[14]T. T. M. Vo, A. J. Williamson, V. Lordi, and G. Galli, Nano Lett. **8**, 1111 (2008).
[15]I. Ponomareva, D. Srivastava, and M. Menon, Nano Lett. **7**, 1155 (2007).
[16]Y. He, D. Donadio, and G. Galli, Nano Lett. **11**, 3608 (2011).
[17]T. M. Gibbons, B. Kang, S. K. Estreicher, and C. Carbogno, Phys. Rev. B **84**, 035317 (2011).
[18]A. Skye, and P. K. Schelling, J. Appl. Phys. **103**, 113524 (2008).
[19]N. Yang, G. Zhang, and B. Li, Nano Lett. **8**, 276 (2008).
[20]Y. Lee, S. Lee, and G. S. Hwang, Phys. Rev. B **83**, 125202 (2011).
[21]J. Garg, N. Bonini, B. Kozinsky, and N. Marzari, Phys. Rev. Lett. **106**, 045901 (2011).
[22]W. Liu and M. Asheghi, J. Appl. Phys. **98**, 123523 (2005).
[23]M. Asheghi, K. Kurabayashi, R. Kasnavi, and K. E. Goodson, J. Appl. Phys. **91**, 5079 (2002).
[24]M. E. Brinson and W. Dunstan, J. Phys. C : Solid State Phys. **3**, 483 (1970).
[25]A. D. McConnell, U. Srinivasan, M. Asheghi, and K. E. Goodson, J. Microelectromech. Syst. **10**, 360 (2001).
[26]P. G. Klemens, Proc. Phys. Soc. London **68**, 1113 (1955).
[27]M. G. Holland, Phys. Rev. **132**, 2461 (1963).
[28]F. Muller-Plathe, J. Chem. Phys. **106**, 6082 (1997).
[29]F. H. Stillinger and T. A. Weber, Phys. Rev. B **31**, 5262 (1985).
[30]Y. Lee and G. S. Hwang, Phys. Rev. B **85**, 125204 (2012).
[31]S. Plimpton, J. Comput. Phys. **177**, 1 (1995).
[32]S. G. Volz and G. Chen, Phys. Rev. B **61**, 2651 (2000).
[33]C. Kittel, *Introduction to Solid State Physics*, 7th Ed. (Wiley, New York, 2006).
[34]F. Schaffler, *Properties of Advanced Semiconductor Materials GaN, AlN, InN, BN, SiC, SiGe*, edited by M. E. Levinshtein, S. L. Rumyantsev, M. S. Shur (John Wiley & Sons, Inc., New York, 2001).
[35]F. Ercolessi and J. B. Adams, Europhys. Lett. **26**, 583 (1994).
[36]Y. Lee and G. S. Hwang (in preparation).
[37]J. P. Perdew and Y. Wang, Phys. Rev. B **45**, 13244 (1992).
[38]G. Kresse and J. Furthmuller, *VASP the Guide* (Vienna University of Technology, Vienna, 2001).
[39]D. Vanderbilt, Phys. Rev. B **41**, 7892 (1990).
[40]J. Che, T. Cagin, and W. A. Goddard III, Nanotechnology **11**, 65 (2000).
[41]J. Che, T. Cagin, W. Deng, and W. A. Goddard III, J. Chem. Phys. **113**, 6888 (2000).
[42]G. A. Slack, Phys. Rev. B **139**, A507 (1965).
[43]B. Abeles, Phys. Rev. **131**, 1906 (1963).